LANGMUIR

pubs.acs.org/Langmuir Article

Bioactives Promiscuity of Mucin: Insight from Multi-Spectroscopic, Thermodynamic, and Molecular Dynamic Simulation Analyses

Komal Kumari, Avinash Kumar, Ahamad Tamanna Manjur, and Surajit Rakshit*

Cite This: *Langmuir* 2023, 39, 4589−4600 Read Online

ACCESS | Metrics & More | Article Recommendations | Supporting Information

ABSTRACT: Mucosal drug delivery plays an increasing role in the clinical setting owing to mucin's advantageous biochemical and pharmacological properties. However, how this transport system recognizes different substrates remains unclear. In this study, we explore the mechanism of bioactive (quercetin and berberine) promiscuity of mucin using various spectroscopic techniques and molecular dynamics simulations. The UV−visible spectroscopy results and the decreased fluorescence intensity of mucin in the presence of the bioactive compounds via a static quenching mechanism confirmed ground-state complex formation between the bioactives and mucin. The binding constants (K_b) were evaluated at different temperatures to afford K_b values of $\sim 10^4$ $Lmol^{-1}$, demonstrating the moderate and reasonable affinity of the bioactives for mucin, yielding greater diffusion into the tissues. Thermodynamic analysis and molecular dynamics (MD) simulations demonstrate that mucin−bioactive complex formation occurs primarily because of electrostatic/ionic interactions, while hydrophobic interactions were also crucial in stabilizing the complex. Far-UV circular dichroism spectroscopy showed that bioactive binding induced secondary structural changes in mucin. Sitemap and MD simulation indicated the principal binding site of mucin for the bioactives. This study also provides insight into the bioactives promiscuity of mucin in the presence of a crowded environment, which is relevant to the biological activity of mucin *in vivo*. An *in vitro* drug release study revealed that crowding assisted drug release in an enhanced burst manner compared with that in a dilute buffer system. This work thus provides fresh insight into drug absorption and distribution in the native cellular environment and helps direct new drug design and use in pharmaceutical and pharmacological fields.

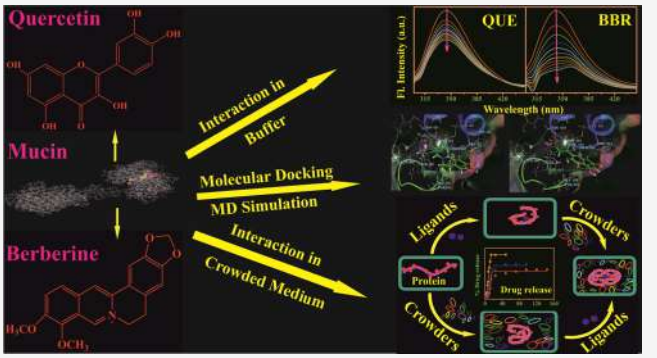

INTRODUCTION

Oral administration is the most attractive approach among the various routes for drug delivery, owing to the use of solid formulations, ease of administration, and enhanced immunological response.[1] The fundamental factors affecting the therapeutic efficacy and bioavailability of an orally administrated drug are the absorption mechanism, distribution through plasma proteins, and nature of the drug. Simultaneously, challenges such as low pH and the mucus barrier are faced during oral delivery, which can denature drugs and prevent their successful absorption into the target, respectively.[2] Consequently, there is a growing demand for new drug delivery methods that provide sufficient contact time at the absorption site. Mucosal delivery has emerged as one of the most studied systems in recent years.[3] This strategy uses the oral route but can also use nasal, ophthalmic, gastrointestinal, and vaginal delivery routes, providing various sites and a vast surface area for drug absorption.[4] In addition, drugs can be easily incorporated near the affected zone with better patient acceptance, affording good targeting and therapeutic efficacy. However, the bioavailability of drugs through mucosal drug delivery depends on various interactions involving the mucosal epithelium surface. Structurally, the mucus layer is a semipermeable viscoelastic hydrogel that protects the underlying epithelium from environmental factors, such as airborne bacteria, pollutants, and pathogenic microorganisms, and forms a potential barrier that drugs must overcome before reaching their site of action and inducing their effect. Therefore, it is crucial to understand how drugs interact with the mucus layer to determine their efficacy and develop new formulations.

The mucus defense activity is mainly due to mucin, a high-molecular-weight *O*-glycosylated protein expressed by epithelial mucus tissues. The major feature of all mucins is a tandem repeat of proline, threonine, and serine residues (PTS domains) and a wide variety of functional groups (fucose,

Received: December 2, 2022
Revised: March 2, 2023
Published: March 14, 2023

https://doi.org/10.1021/acs.langmuir.2c03268
Langmuir 2023, 39, 4589−4600

galactose, sialic acid, and *N*- and *O*-linked oligosaccharides) in its structure. In addition to its protective functions, the aberrant expression or glycosylation of mucin can cause various diseases, such as cancer, cystic fibrosis, asthma, and chronic obstructive pulmonary diseases, which has established mucin as an important marker of adverse prognosis and an attractive therapeutic target in recent years.[5,6] Along with the defensive function of mucin, studying the diffusion/interaction of molecules such as nutrients and enteric drugs through mucin has substantial physiological importance and is key in designing drugs that must be absorbed and gain access to the circulatory system and distribution or be kept from entering it. For instance, Boegh et al. studied the mucus permeability of peptides and proteins and found that mucus is the primary barrier against the bioavailability of oral drugs.[7] Alternatively, the inner mucus layer is known to assist the uptake efficiency of drugs, justifying the dual role of mucus in the absorption/desorption of orally administrated drugs.[8,9]

The idea of using mucin to simulate mucus is somewhat oversimplified and well documented in the literature.[10−12] However, this approach may provide important information regarding the interactions that take place between drugs and mucin. For example, Visentin et al. recently studied the interaction between mucin and different drugs used in the treatment of cystic fibrosis via spectroscopic approaches.[12,13] Yi et al. studied the interaction between oxymetazoline hydrochloride, a selective α-1, and mucin using fluorescence spectroscopic techniques.[14] Currently, there remains no conclusive understanding of the nature of the molecular interactions between drug molecules and mucin in *in vivo* scenarios that can be drawn from the existing literature. Thus, a systematic study of the substrate promiscuity characteristics of mucin is needed to clarify the role of mucin in drug absorption, diffusion, and redistribution in both *in vitro* and *in vivo* scenarios. In this context, this work performed a systematic study of the interactions between mucin and two bioactive drugs, quercetin (QUE) and berberine (BBR), using various spectroscopic techniques with the variation of pH and temperature as well as molecular docking, and molecular dynamics (MD) simulation techniques, and the presence of crowding agents that mimic *in vivo* scenarios.

Bioactive drugs have begun to push the frontiers of biochemical and biological research owing to their extensive medicinal and pharmaceutical applications. BBR is an isoquinoline alkaloid (Scheme 1), an important traditional medicinal herb isolated from *Berberis vulgaris*, *Hydrastis canadensis*, and *Captis chinensis* and has been found to have analgesic, antibacterial, antimalarial, antitubercular, antileishmanial, and antitumor activities *in vitro* and *in vivo*.[15−19] QUE is the most abundant naturally occurring flavonoid (Scheme 1) and is found to inhibit the activities of calcium/phospholipid-dependent protein kinase, DNA topoisomerases, and the growth of leukemia cells, Ehrlich ascites, and NK/Ly ascites tumor cells.[20−22] Moreover, QUE has been shown to reduce expression of MUC5AC, mainly induced by neutrophil elastase in airway epithelial cells (HBE16), at both RNA and protein levels through the PKC/EGFR/ERK signal transduction pathway.[23] BBR has been shown to increase mucin release by directly acting on airway mucin-secreting cells, which suggests that these agents can be further studied for possible use as mild expectorants during the treatment of chronic airway diseases.[24] Despite significant information on the medicinal potential of BBR and QUE, the molecular mechanism of the bioactives promiscuity characteristics of mucin as well as details of the complete efflux process remain unclear. A better understanding of the nature and mechanism of interactions between the different classes of bioactives with mucin could suggest new approaches to drug therapy and design and their importance in pharmacology and pharmacodynamics. Macromolecular crowding is an important parameter that allows for the fine control of different biophysical properties (protein folding/unfolding, compaction, aggregation, etc.) in *in vivo* systems compared with those in dilute *in vitro* systems, although the impact of macromolecular crowding in the study of protein−drug interactions has rarely been studied. In this regard, the study of protein−bioactive interactions in a crowded milieu is an interesting subject to explore the impact of bioactive promiscuity (absorption, diffusion, and redistribution) of mucin in the cellular environment. We also examined the influence of pH on the structure−function characteristics of mucin and sought to identify mucin behavior at different pH values toward bioactive absorption.

Scheme 1. Molecular Structures of Berberine and Quercetin

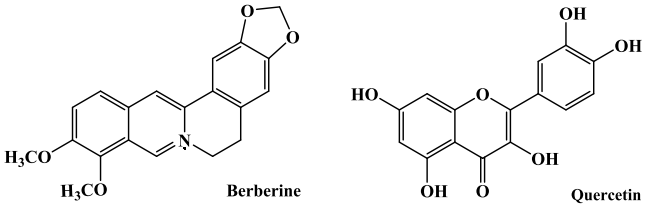

EXPERIMENTAL SECTION

Chemicals. Berberine chloride hydrate and quercetin hydrate were purchased from TCI Chemicals. Mucin from the porcine stomach (Type III), sodium phosphate dibasic, sodium phosphate monobasic, Ficoll 70, and Ficoll 400 were purchased from Sigma-Aldrich. All of the chemicals were used as received, without further purification.

Solution Preparation. Mucin solutions were prepared using double-distilled water by dissolving porcine stomach mucin in appropriate buffer solutions. Three buffer solutions (0.1 M) using citrate buffer (pH 3.0), acetate buffer (pH 5.0), and phosphate buffer (pH 7.4) were used to maintain the pH. Concentrated stock solutions of the bioactives were prepared by dissolving them in buffer at different pH values. Aliquots from the stock solutions of the bioactive compounds were added to mucin solutions to achieve the final bioactive concentrations. The concentrations of the protein and the bioactive used in different experiments have been specified in context of the relevant discussion.

Spectroscopic Measurements. Steady-state absorption and emission were measured with a V-730 UV−visible spectrophotometer and an FP-8200 spectrofluorometer (Jasco, Tokyo, Japan), respectively, with a temperature controller attachment from ESCY (IC201) using 0.1 mg/mL mucin with successive additions of bioactives solutions at different concentrations: over a range from 0 to 50 μM for QUE and from 0 to 10 μM for BBR. Circular dichroism (CD) measurements were performed on a Jasco 1500 spectropolarimeter at a protein concentration of 0.2 and 0.6 mg/mL for far-UV and near-UV, respectively, using a quartz cuvette with a path length of 0.1 cm.

Molecular Docking Studies. Molecular modeling studies were performed using the Maestro (v 11.4) panel from Schrodinger, Inc. Prior to performing the molecular modeling simulations, the solution structures of QUE and BBR (in the SMILES format) were imported into the workspace and prepared using the Ligprep tool in the Maestro interface. The chirality of the ligands was corrected and their

https://doi.org/10.1021/acs.langmuir.2c03268
Langmuir 2023, 39, 4589−4600

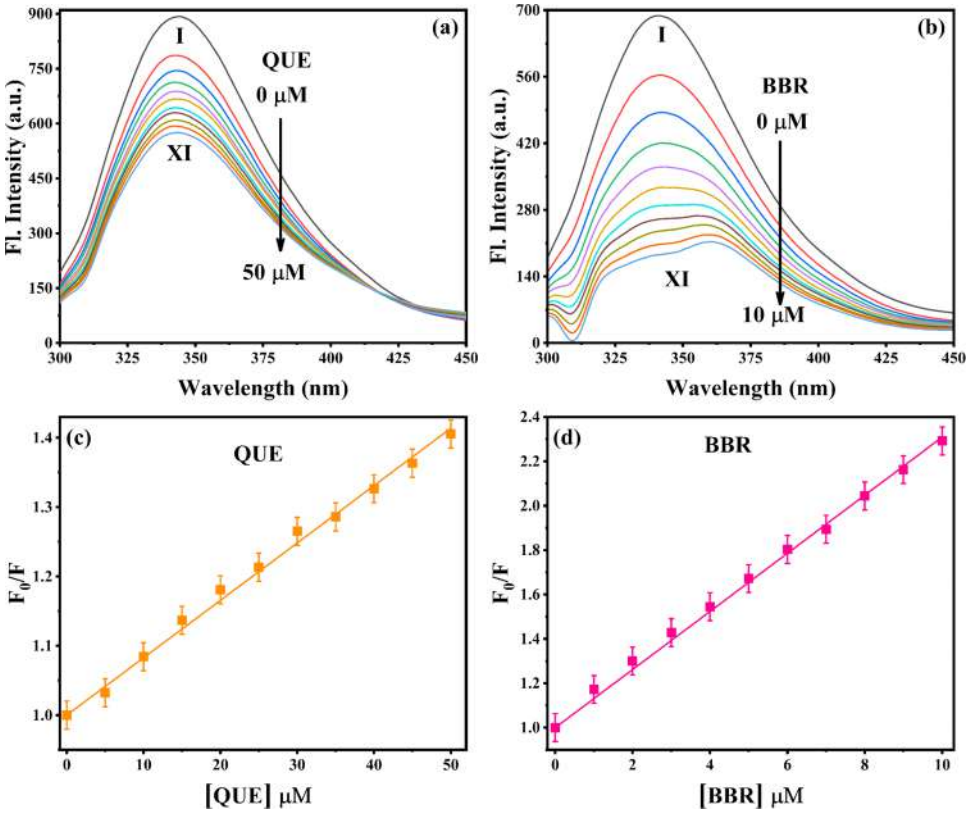

Figure 1. (a, b) Emission spectra of mucin (0.1 mg/mL) in the absence and presence of bioactives (QUE and BBR) at different concentrations. (a) Curves (I–XI) represent 0, 5, 10, 15, 20, 25, 30, 35, 40, 45, and 50 μM QUE, respectively. (b) Curves (I–XI) represent 0, 1, 2, 3, 4, 5, 6, 7, 8, 9, and 10 μM BBR, respectively. Stern–Volmer plots of the fluorescence quenching of mucin by (c) QUE and (d) BBR.

3D structures in the lowest energy state were generated at neutral pH by employing the OPLS3e force field.[25] The X-ray crystal structure of mucin was retrieved from the protein data bank (PDB ID: 7PP6 and 6RBF).[26] This was then used for refining with the protein preparation wizard (PPW) tool of Maestro. PPW has a streamlined workflow divided into three steps. Import and process was the first step, where hydrogen atoms were added, the bond order was assigned, zero-order bonds to metals were created, disulfide bonds were created, selenomethionines were converted to methionines, the side chains and missing loops were completed using Prime and water molecules beyond 5 Å of the hetero atoms were deleted. Next, the structure was reviewed and modified. Refining was completed using PROPKA, the hydrogen atoms were optimized, and restrained minimization using the OPLS3e force field was performed.[25] Grid generation was then required as the molecular docking algorithm in Glide is a grid-based docking system. However, because the PDB lacks a mucin-ligand co-crystallized structure, the sitemap tool of Maestro was used to predict the possible binding site. Sitemap joins together different site points that are contributed by probable protein–protein or protein–ligand binding preferably closer to the surface of the protein and with the nonexposed part toward the solvent. Any smaller sites that are closely adjacent to one another can be merged into one large site point. Finally, the predicted sites are ranked based on their D-score and site score, where the D-score indicates the draggability of the predicted site.[27] A receptor grid was generated based on the amino acid residues present in the highest-ranked active site. Based on the receptor grid, QUE and BBR were docked in the extra-precision mode (XP) in the Glide module.[28]

MD Analysis. MD simulations of mucin 2 (PDB ID: 7PP6) complex with bioactives were performed using GROMACS for 50 ns. The PDB ID 7PP6 is a cryo-electron structure of MUC2 tubules of the D1, D2, and D3 domains. The simulation was completed using GROMACS 2018.3 on a LINUX system with NVIDIA GPU support.[29] AMBER ff99SB-ILDN was employed as the force field and tip3p was used as the water model. The Antechamber tool of AMBERTOOLS was employed to generate the ligand topology. The system was neutralized by adding sodium and chloride ions. The conjugate gradient and steepest descent algorithm were employed successively for energy minimization. Then, 2-phase equilibration was completed, each for 100 ps at time steps of 2 fs. Finally, the well-equilibrated system at a temperature of 300 K and 1 bar pressure was released for position restraint to run the MD simulation for 100 ns with a time step of 2 fs. The LINCS algorithm was used for holonomic constraints and the Verlet cutoff scheme was selected for neighbor searching. vdW and PME were used for electrostatics calculations. The GROMACS in-built tools were used to perform the analysis and Xmgrace was used to plot the data.

In addition to rendering the MD simulation of QUE and BBR with mucin 2 (PDB ID: 7PP6) using GROMACS, we performed MD simulation with the D3 domain of mucin only (6RBF) using the Desmond module.[30] Desmond has a three-step integrated workflow, wherein the first step, the protein–ligand complex is solvated, neutralized by adding counter ions, and the boundary is defined. Herein, SPC (simple point to charge) was used as the solvent model in an orthorhombic box and Na^+ ions were added to neutralize the system. In the next step, the solvated complex was minimized and finally submitted for MD simulation at 20,000 ps at 300 K and 1.01325 bar pressure. The protein–ligand complex was used in binding free energy calculations (MM-GBSA) by employing the Prime module in the Maestro panel.[31]

***In Vitro* Drug Release Study.** To evaluate the kinetics of bioactive release from the mucin–bioactive complex, *in vitro* drug release was explored in the absence and presence of the crowding agent (4% Ficoll 400), and free bioactives served as a control. Typically, a 1 mL sample solution of the mucin–bioactive complex in a 1:1 ratio (with or without 4% Ficoll 400) was transferred into a dialysis tube with a molecular weight cutoff of 8000 Da and then dialyzed against the release medium containing phosphate-buffered

https://doi.org/10.1021/acs.langmuir.2c03268
Langmuir 2023, 39, 4589–4600

Table 1. Stern-Volmer Quenching Constants (K_{SV}), Bimolecular Quenching Constant (Kq), Binding Constants (K_b), and Binding Sites (n) of the Mucin and Bioactive Interactions

drug	K_{sv} (M^{-1})	K_q ($M^{-1}S^{-1}$)	K_b (M^{-1})	n
QUE	8.3×10^3 (±0.01)	8.3×10^{11} (±0.01)	3.0×10^3(±0.03)	1.33
BBR	1.3×10^5 (±0.01)	1.3×10^{13} (±0.01)	4.9×10^4 (±0.02)	1.26

Table 2. Quenching Constants (K_{SV}), Binding Constants (K_b), Binding Stoichiometry (n), and Thermodynamic Parameters between Mucin and the QUE and BBR Bioactives at Different Temperatures Obtained from Fluorescence Quenching Experiments

	T (K)	K_{SV} (M^{-1})	K_b (M^{-1})	n	ΔG^0 ($kJmol^{-1}$)	ΔH^0 ($kJmol^{-1}$)	ΔS^0 ($Jmol^{-1}K^{-1}$)
QUE	283	9.1×10^3 (±0.01)	3.3×10^3 (±0.03)	1.33	−19.15	−15.41	13.23
	293	8.4×10^3 (±0.02)	3.1×10^3 (±0.04)	1.34	−19.28		
	303	6.2×10^3 (±0.01)	2.0×10^3 (±0.07)	1.35	−19.42		
	313	5.6×10^3 (±0.01)	1.9×10^3 (±0.07)	1.33	−19.55		
BBR	283	1.6×10^5 (±0.01)	5.0×10^4 (±0.02)	1.27	−25.52	−6.40	67.55
	293	1.4×10^5 (±0.01)	4.9×10^4 (±0.02)	1.26	−26.20		
	303	1.0×10^5 (±0.008)	4.3×10^4 (±0.06)	1.24	−26.87		
	313	0.9×10^5 (±0.008)	3.9×10^4 (±0.06)	1.22	−27.55		

saline (100 mL; pH 7.4) with constant stirring at a speed of 200 rpm. The release media was collected at predetermined intervals, and new release media was added to maintain the sink conditions. The released bioactive concentration was determined by UV−visible spectrophotometry at 336 nm for BBR and 381 nm for QUE.

RESULTS

Steady-State Absorption and Fluorescence Spectroscopy Study. To explore the bioactives promiscuity of mucin, UV−visible absorption and fluorescence spectroscopy were used to study the interaction behavior. The absorption and emission spectra of mucin were recorded after the progressive addition of the bioactives at a constant concentration of mucin (0.1 mg/mL) (Figures 1a,b and S1). Mucin absorbs at a peak at ∼260 nm, which is mostly due to the amino acid phenylalanine. The intrinsic fluorescence of mucin at ∼345 nm is mainly due to the tryptophan residue as phenylalanine has a considerably low fluorescence yield and a significant quenching of tyrosine fluorescence as a consequence of the presence of amino acids in the near vicinity or an efficient energy transfer to tryptophan moiety. With an increase in the concentration of BBR and QUE, quenching is seen in the fluorescence spectrum of mucin implying the complex formation via noncovalent interactions.[32,33] However, this quenching may be due to the inner filter effect as the QUE and BBR in the buffer have significant absorption in the emission range of mucin (300−450 nm) (Figure S28).[34,35] Thus, the fluorescence quenching data were evaluated after correcting the fluorescence intensities using eq S1. Furthermore, when the QUE concentration was increased from 0 to 50 μM, a bathochromic shift from 360 to 363 nm occurred in the maximum emission wavelength of the protein. A similar observation has been found with the addition of BBR, i.e., a decrease in the fluorescence intensity and a shift in the maximum emission wavelength of mucin from 360 to 375 nm in the presence of 0−10 μM BBR. This suggests increased hydrophilicity of the region surrounding the tryptophan site.

Binding Mechanism. The binding mechanism was assessed by evaluating the fluorescence quenching using the Stern−Volmer equation

$$F_0/F = 1 + K_q\tau_0[Q] = 1 + K_{sv}[Q] \quad (1)$$

where F_0 and F are the fluorescence intensities of the protein in the absence and presence of bioactives, respectively, [Q] is the quencher (bioactive) concentration, K_{SV} is the Stern−Volmer quenching constant, K_q is the bimolecular quenching constant, and τ_0 is the lifetime of the fluorophore in the absence of quencher and approximately 10^{-8} for a tryptophan residue.[36] Figure 1c,d shows that, within the investigated concentration range, the linearity of the fluorescence ratio is in good agreement with the Stern−Volmer equation, indicating a single quenching type (static or dynamic), and the corresponding results are summarized in Table 1. The quenching constants (K_q) were calculated to be 8.3×10^{11} and 1.3×10^{13} M^{-1} s^{-1}. The K_q value of mucin quenching initiated by bioactives was much greater than 2×10^{10} M^{-1} s^{-1}, the maximum diffusion collision quenching rate constant of various drugs with proteins. This indicated that the quenching is initiated by the formation of a ground-state complex or static type.

Binding Constant and Binding Sites. The fluorescence data were further assessed to determine the binding constant and the number of binding sites by following the modified Stern−Volmer equation

$$\log\left(\frac{F_0 - F}{F}\right) = \log\ K_b + n \log\ [Q] \quad (2)$$

where F_0 and F stand for the fluorescence intensity of the protein in the absence and presence of bioactives, respectively, [Q] is the concentration of the quencher, and K_b denotes the binding constant of bioactives with the protein in the quenching process. Figure S2 illustrates the linear dependence of $\log[(F_0 - F)/F]$ on $\log$ [Q] for each complex. The binding constant was in the order of 10^4 ($Lmol^{-1}$) showing moderate and reasonable binding,[12,13] while the near-unity value of n (n = 1.33 for QUE and n = 1.26 for BBR) implies that each ligand (QUE and BBR) is bound in a single site on mucin (Table 1).

Thermodynamic Parameters and Nature of the Binding Forces. To improve the understanding of the thermodynamics (change in enthalpy and entropy) of the complex formation and the type of interaction forces between the bioactives and mucin, fluorescence titration spectra were recorded and the binding constant was determined at several temperatures according to the modified Stern−Volmer equation (Figures S3−S6). Considering the minimal variation

https://doi.org/10.1021/acs.langmuir.2c03268
Langmuir 2023, 39, 4589−4600

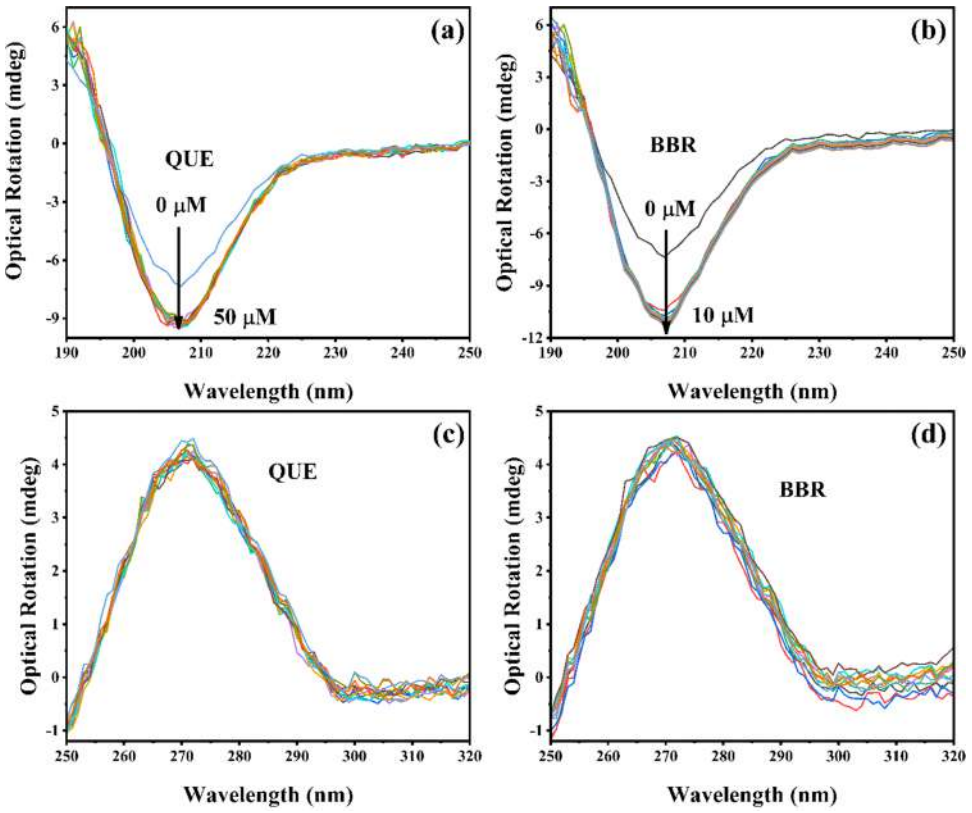

Figure 2. (a, b) Far-UV and (c, d) near-UV CD spectra of mucin in the presence of varying concentrations of bioactives added in phosphate buffer of pH 7.4 at 298 K.

of the enthalpy change (ΔH^0) within the studied temperature range, enthalpy change (ΔH^0) and entropy change (ΔS^0) of formation of the QUE–mucin and BBR–mucin complexes were estimated according to the van't Hoff equation[12−14,36]

$$\ln K_b = -\Delta H^0/RT + \Delta S^0/R \quad (3)$$

Here, R is the universal gas constant and T is the temperature in Kelvin. The enthalpy change (ΔH^0) and entropy change (ΔS^0) are calculated from the slope and intercept of the van't Hoff plots (Figure S7).

The free energy change (ΔG^0) of the process is then calculated from the following relationship

$$\Delta G^0 = -RT \ln K_b = \Delta H^0 - T\Delta S^0 \quad (4)$$

where K_b is the binding constant at the corresponding temperature (T), R is the gas constant, and ΔG^0, ΔH^0, and ΔS^0 are the changes in the standard free energy, enthalpy, and entropy, respectively. The calculated values of the thermodynamic parameters (ΔH^0, ΔS^0, *and* ΔG^0) are listed in Table 2.

CD Study. To investigate the structural and conformational changes in mucin upon interaction with the bioactive, the far-UV and near-UV CD spectra of mucin recorded in the presence of various concentrations of bioactive are shown in Figure 2. The negative absorption band at 206 nm in far-UV CD (Figure 2a,b) reveals that the majority of the secondary structure of mucin appears to be random coils with no detectable features of α-helices or β-sheets, as the vast majority of the polypeptide backbone is heavily glycosylated.[37,38] As is evident from the figure, increasing bioactive concentration accompanies an increase of CD signal, indicating the conformational change in mucin secondary structure upon interaction with the bioactives. To quantitatively analyze the secondary structure changes of mucin, secondary structure components are calculated on the basis of raw CD data listed in Table 3. However, with further increasing the bioactive concentration, the optical rotation almost remains unaltered indicating the stability of the complex. Figure 2c,d displays the near-CD features of mucin with maxima at ∼270 nm corroborating the presence of phenylalanine. Upon increase in the bioactives concentration, no significant change in the near-UV CD spectrum is observed, indicating that the tertiary structure of the mucin is preserved upon binding with bioactives.

Table 3. Secondary Structural Analysis of the Mucin and Mucin–Bioactive Systems from the CD Data at pH = 7.4 and T = 298 K

system	α-helix (%)	β-sheet (%)	random coil (%)
mucin	6.2	31.8	62.1
mucin–QUE	10.1	28.1	61.7
mucin–BBR	8.8	32.9	58.3

Molecular Docking Analysis. Molecular docking analysis can predict the binding mode between a ligand and a binding site in a macromolecule. Therefore, we studied the binding interactions of the bioactive with mucin (PDB ID: 7PP6) as predicted by molecular docking analysis. Using the sitemap tool, a total of five possible sites were predicted (Table S2) and based on the site score and D-score, Site 1 was selected as the most promising active site for further docking studies (Figure S9). Based on the amino acid residues present in the active site (Site 1), bioactives preferably bind in the D3 domain of the

https://doi.org/10.1021/acs.langmuir.2c03268
Langmuir 2023, 39, 4589−4600

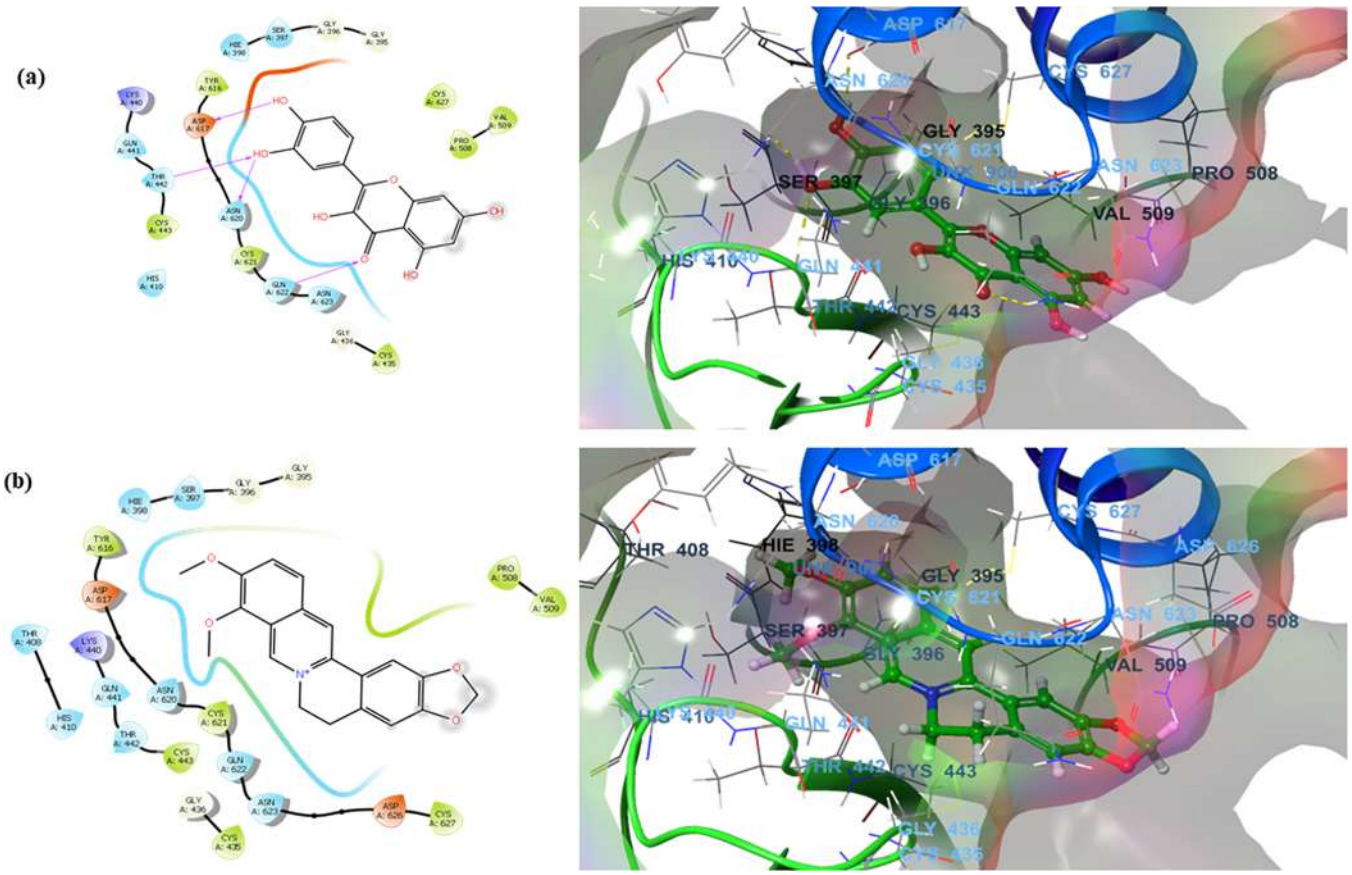

Figure 3. Ligand interaction diagram of Mucin 2 (PDB ID: 7PP6) with (a) QUE and (b) BBR.

protein. Both the compounds showed favorable docking scores and several non-bonding interactions, suggesting that they might bind well with mucin. QUE showed a docking score of −8.775 kcal/mol, exhibiting potential for H-bonding interactions with THR442, ASP617, ASN620, and GLN622 residues (Figure 3a). Other active site residues were hydrophobic in nature from that of Tyr 616 more closely with the QUE and play a significant role in fluorescence quenching. On the other hand, BBR exhibited a docking score of −6.825 kcal/mol showing mainly hydrophobic interactions with the active side residues along with polar, charged-positive, and charged-negative interactions (Figure 3b). To gain more information about the binding mode of bioactives in mucin, molecular docking analysis with only the D3 domain of mucin (PDB ID: 6RBF) was performed using the Desmond module (see the Supporting Information).

MD Analysis. The MD simulation was performed to understand the bioactives stability and behavior in the mucin system. After the docking, the best binding pose of bioactives in mucin was taken for MD simulation using GROMACS. The RMSD values of C-α atoms were measured with respect to the first frame (Figure S12). For the BBR−receptor complex (black line) equilibrium was attained at ∼3 ns and then maintained with intermittent deviations of 0.3−1.0 nm. The QUE−receptor complex (red line) also attained equilibrium at around 3 ns and then remained stable with intermittent deviations of 0.3−1.5 nm. There was more deviation with the QUE−receptor complex than with the BBR complex, however, both of these stabilized during the last 8 ns of the simulation period. Solvent-accessible surface area (SASA) is another parameter to examine the extent of exposure of proteins to the surrounding solvent molecules, as binding of the ligand may induce the conformational changes in the protein and hence the area in contact with the solvent also may vary. The SASA values of the QUE−receptor complex (red) and BBR−receptor complex (black) were plotted against time to estimate the changes in surface area (Figure S13). The trajectory for the SASA complex indicated a decrease in the values up to 20 ns. The average SASA value was found to be 370 nm^2 and was between 350 and 390 nm^2. Overall, the analyses revealed that the surface area of protein in complexes was shrunken during the simulation. Further, the Radius of gyration (R_g), Root Mean Square Fluctuation (RMSF), and hydrogen bonds analysis was also performed for the 50 ns trajectory period (Figure S14−16). R_g is an important parameter to find out the overall change in the protein structure compactness and its dimensions during the simulation. The binding of bioactives decreased the backbone R_g values, suggesting that the structure is getting more compact after the ligand binding.

For better understanding, we have performed the MD simulation with the D3 domain of mucin using the Desmond tool. The MD simulation was performed for 20,000 ps, and a frame was captured every 20 ps, to generate a total of 1000 frames. All of the frames were aligned over the first frame and the root mean square deviation (RMSD) was calculated. RMSD values reflect the stability of the protein−bioactive complex and a deviation of <3Å is considered stable.[39] The RMSD deviations for the BBR−mucin and QUE−mucin complexes were <2Å throughout the simulation (Figures S17 and S18). The complex drifted together for the whole

https://doi.org/10.1021/acs.langmuir.2c03268
Langmuir 2023, 39, 4589−4600

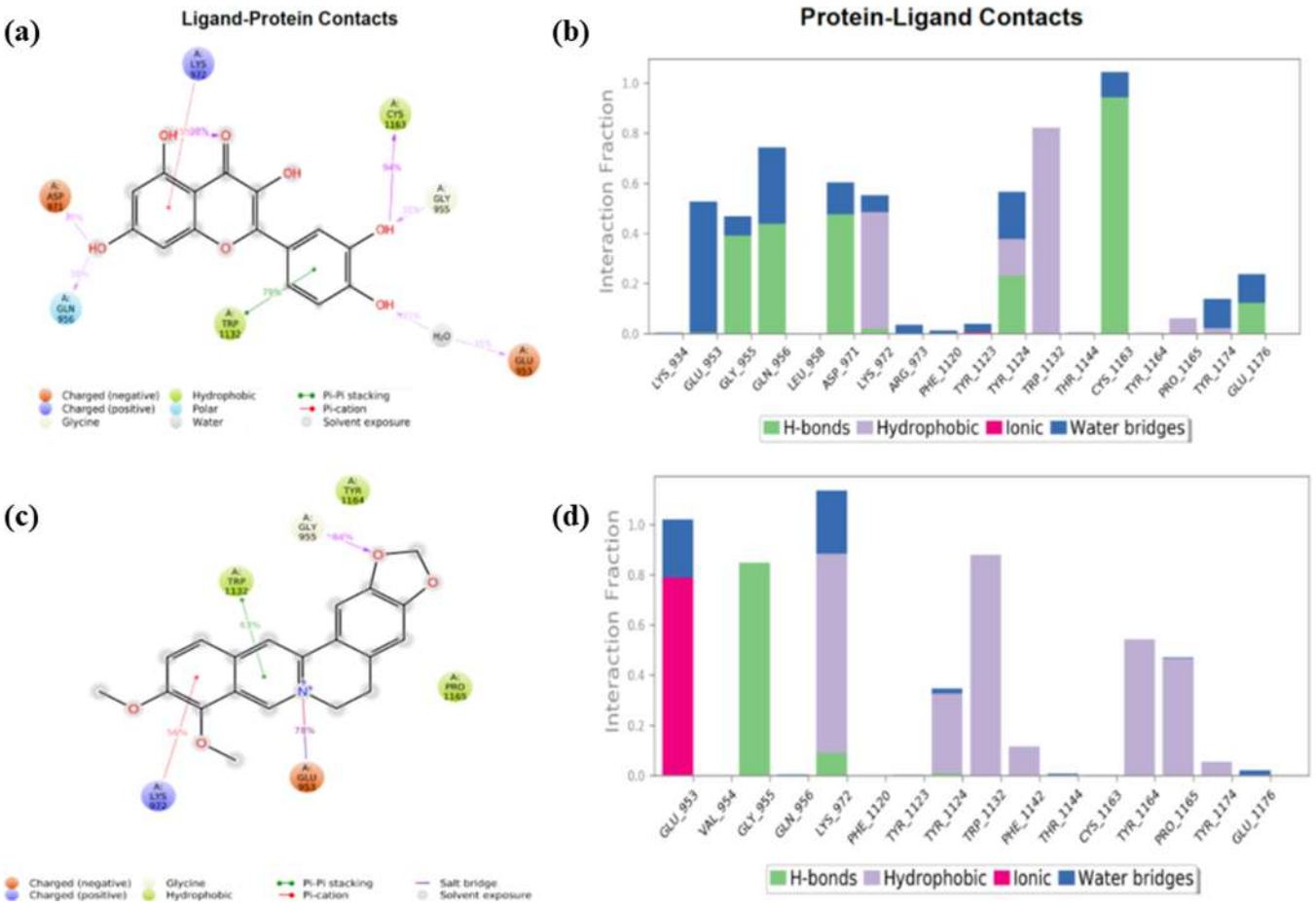

Figure 4. 2D ligand interaction diagram for the (a) QUE−mucin and (c) BBR−mucin complex. Histogram plot for the (b) protein−QUE and (d) protein−BBR contacts (PDB ID: 6RBF).

simulation period, suggesting the stability of both complexes. A slight deviation was observed between 17 to 17.5 ns in the BBR system and 10−12.5 ns in the QUE system but after that, the complex stabilized again toward the end of the simulation period. A histogram and 2D- ligand interaction diagram was plotted to assess the duration of the corresponding non-bonding interactions and whether any new interaction was observed in comparison to the XP docking poses (Figure 4). The H-bonding interaction with GLY955 was observed during docking studies and was evident for 84% of the simulation time during MD studies (Figure 4c). The π-cation interaction with LYS972 was observed for 56% of the simulation time while $\pi-\pi$ stacking interaction with TRP1132 was observed for 63% of the simulation time. Ionic interaction was observed with GLU953 78% of the time. A hydrophobic interaction was observed in the QUE system with LYS972 and TRP1132 for 98 and 79% of the stimulation time, respectively. H-bonding interaction with the CYS1163 residue was found for 94% of the simulation time (Figure 4a). The histogram plot in Figure 4b,d shows several water bridges being formed with GLU953 and LYS972 for BBR, whereas LYS934, TRP1174, GLU953, and ARG973 are involved in water bridge formation in the QUE system.

Effect of Cobinding of Bioactive to Mucin. Based on the molecular docking analysis, we found that both the bioactives preferably bind with the D3 domain of mucin. Therefore, we have studied the cobinding of both bioactives with mucin as cobinding can affect the free biologically active fraction in the *in vivo* scenario. We observed the effect of cobinding of bioactives with mucin in two ways: (i) first, we prepared a mucin−BBR complex at a particular ratio followed by increasing the QUE concentration from 1 to 50 μM; (ii) in the second case, we prepared a mucin−QUE complex at a particular ratio followed by increasing the BBR concentration from 1 to 10 μM. Biochemical parameters of bioactive cobinding to the D3 domain of mucin were determined according to the Stern−Volmer and modified Stern−Volmer equations (Figure S27 and Table S4).

Effect of pH on Bioactive Binding to Mucin. The pH-induced drug binding mechanism plays an important role in drug absorption and bioavailability as this has a significant influence on drug dissolution, release, and cellular permeability. Previous structural and dynamic studies developed a model for the pH-induced protective barrier properties of mucin.[40−42] For example, porcine gastric mucin (PGM) solution shows a 100-fold increase in viscosity when the pH is lowered from 7 to 2.[43] HCl secreted by the gastric gland can penetrate the mucus gel layer through narrow fingers when the pH of the PGM solution is >5, while HCl is unable to penetrate when the pH is <4.[40] Similarly, the binding of *H. pylori* strain SVA 40 to mucin is dependent on pH and the degree of sulfation of mucin, with stronger binding at low pH (<3) to highly sulfated mucin at high pH (pH = 4−7.4) to low sulfated mucin.[41] These pH-dependent observations directed us to study the impact of pH on mucin-drug interactions. Therefore, to understand the role of pH on bioactive

https://doi.org/10.1021/acs.langmuir.2c03268
Langmuir 2023, 39, 4589−4600

absorption, we investigated the binding between the BBR and QUE bioactive and mucin under different pH conditions (3.0, 5.0, 7.4) and determined the binding parameters according to the Stern−Volmer and modified Stern−Volmer equations (Figures S19−S21) are summarized in Table 4.

Effect of Macromolecular Crowding on Bioactive Binding to Mucin. Within the cells, proteins are generally influenced by a densely crowded, heterogeneous, and complex environment that can affect their stability, conformation, and ligand binding propensity.[44−47] However, most experimental studies on protein−drug interactions focus on macroscopic properties, such as stability, diffusion, and binding affinity, while the local effects of crowding have been largely overlooked. Recently, Chen et al. reported that bovine serum albumin displayed an increased binding constant for saturated medium-chain fatty acids with increased crowding but a significantly decreased binding constant for unsaturated long-chain fatty acids in crowded environments. Therefore, it is essential to determine the effect of crowding on the interaction of mucin with the bioactive.

Here, we investigated the crowding effect in mucin and bioactive binding using Ficoll 70 and 400 as molecular crowder. We observed the effect of crowding on the mucin−bioactive interaction in two ways: (i) first, we prepared a mucin−bioactive complex at a particular ratio followed by increasing the crowder concentration from 0 to 20%; (ii) in the second case, the protein was kept at the same crowder concentration but the bioactive concentrations were varied. The mucin−bioactive binding parameters were determined according to the Stern−Volmer and modified Stern−Volmer equations (Figures 5, S23−25) are summarized in Table 5.

Drug Release Study. To elucidate the role of mucin as a natural barrier in mucosal drug delivery, a drug carrier diffusion study was designed followed by the mucin-drug interaction in the dilute and crowded medium. An *in vitro* release study of the bioactive from the mucin−bioactive complex under physiological conditions (pH 7.4) in the absence and presence of crowding agents was performed using free bioactive sealed in a dialysis bag for comparison. Figure 6 shows the *in vitro* release kinetics exhibited by the bioactive from the mucin−bioactive complex in the presence and absence of the crowding agent (Ficoll 400). The maximal release percentages were fitted through the commonly used release kinetic equations and found that Weibull models can describe the release profiles with good fitting.

DISCUSSION

The interaction of drugs with mucin in mucosal drug delivery plays a key role in determining the absorption, distribution, activity, and rate of excretion of drugs in the body. Therefore, in this study, we focused on the bioactives promiscuity of mucin by unmasking the binding affinity, binding patch, nature of interaction, mechanism, and drug release study in both dilute and crowded environments using various spectroscopic techniques and molecular dynamics simulations.

Fluorescence spectroscopy is a powerful tool for the study of determining interactions between small molecules and biomacromolecules. As demonstrated in Figure 2a,b, increasing bioactive concentration markedly decreased the intensity of mucin fluorescence with a bathochromic shift in λ_{em}, indicating the formation of a mucin−bioactive complex and the change in the solvent polarity of tryptophan microenvironment of mucin during the binding interaction.[12,13,33,48] This is in concordance

Table 4. Binding Constants (K_b), Quenching Constants (K_{SV}), and Binding Sites (n) of the Mucin and Bioactive Interactions at Different pH Values

pH	7.4			5.0			3.0		
drug	K_{sv} (M^{-1})	K_b (M^{-1})	n	K_{sv} (M^{-1})	K_b (M^{-1})	n	K_{sv} (M^{-1})	K_b (M^{-1})	n
QUE	8.3×10^3 (±0.01)	3.0×10^3 (±0.03)	1.33	8.8×10^3 (±0.01)	3.1×10^3 (±0.04)	1.35	9.4×10^3 (±0.01)	3.9×10^3 (±0.04)	1.35
BBR	1.3×10^5 (±0.002)	5.0×10^4 (±0.01)	1.26	1.2×10^5 (±0.002)	4.8×10^4 (±0.01)	1.23	1.0×10^5 (±0.002)	4.7×10^4 (±0.03)	1.43

https://doi.org/10.1021/acs.langmuir.2c03268
Langmuir 2023, 39, 4589−4600

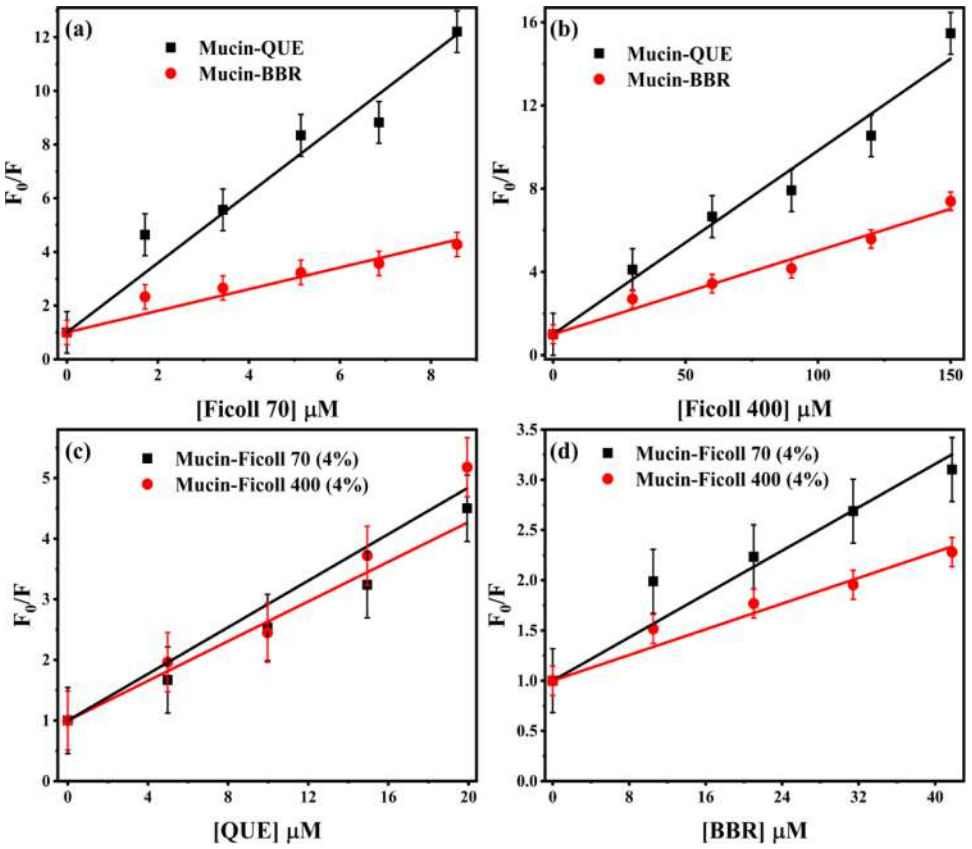

Figure 5. Stern−Volmer plots of the mucin−bioactive complex (mucin = 0.1 mg/mL; QUE = 1 μM; BBR = 0.5 μM) at various concentrations of (a) Ficoll 70 and (b) Ficoll 400. Stern−Volmer plots of mucin at various concentrations of (c) quercetin and (d) berberine while keeping the crowder concentration at 4%.

Table 5. Binding Parameters of the Mucin−Bioactive Complex (A) at a Fixed Crowding Agent Concentration (4%) and (B) at a Fixed Bioactive Concentration ([QUE] = 1 μM and [BBR] = 0.5 μM). The Mucin Concentration Was Kept Constant at 0.1 mg/mL in Both Cases

	K_{sv} (M^{-1})	K_b (M^{-1})	n	K_{sv} (M^{-1})	K_b (M^{-1})	n
A		Ficoll 70			Ficoll 400	
QUE	0.21×10^3 (±0.01)	6.9×10^{10} (±0.31)	0.55	0.41×10^3 (±0.03)	3.63×10^8 (±0.91)	0.61
BBR	0.06×10^3 (±0.01)	1.34×10^7 (±0.06)	0.63	0.09×10^3 (±0.01)	5.74×10^6 (±0.09)	0.54
B		QUE			BBR	
Ficoll 70	1.45×10^3 (±0.10)	2.29×10^3 (±0.11)	0.68	0.56×10^3 (±0.07)	0.93×10^3 (±0.07)	0.54
Ficoll 400	0.10×10^3 (±0.01)	1.44×10^2 (±0.19)	0.61	0.05×10^3 (±0.01)	1.03×10^2 (±0.22)	0.59

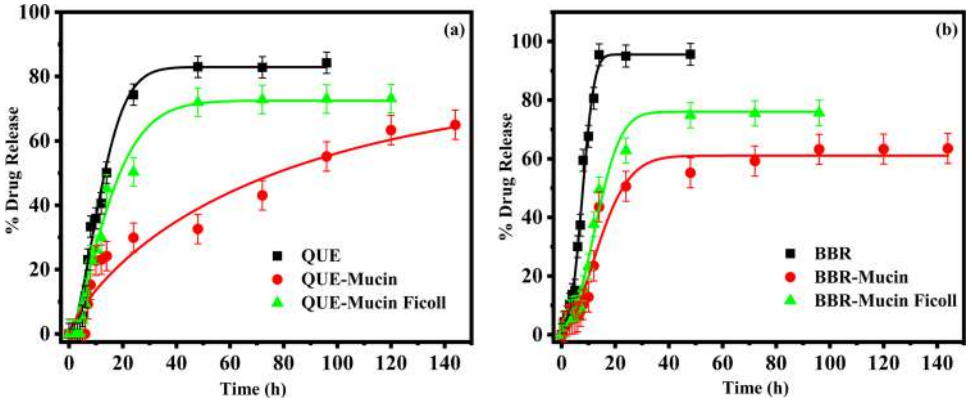

Figure 6. Release profile of (a) QUE and (b) BBR in phosphate buffer *in vitro* (-■- free bioactive; -▲- mucin−bioactive complex; -●- mucin−bioactive complex in the presence of a crowder). (Solid lines are best fit to the experimental data).

https://doi.org/10.1021/acs.langmuir.2c03268
Langmuir 2023, 39, 4589−4600

with far-UV CD results exposed above. The decrease in the K_{SV} of the mucin−bioactive complex with increasing temperature indicates static quenching between mucin and the bioactive molecules as the increase in temperature tends to disfavor the binding interaction (Table 2). The K_b values suggest the formation of a moderately bound complex of bioactives with mucin, indicating the higher diffusion of the bioactives into the tissues through the mucosal route. Thermodynamic parameters were calculated to decipher the underlying mechanistic aspects of the mucin−bioactive interaction process according to the Ross model.[12−14,36] Briefly, based on the thermodynamic data, the mode of interaction can be (i) $\Delta H > 0$, $\Delta S > 0$ correspond to hydrophobic forces; (ii) $\Delta H < 0$, $\Delta S < 0$ correspond to van der Waals interaction, hydrogen-bond formation; and (iii) $\Delta H < 0$, $\Delta S > 0$ correspond to electrostatic/ionic interactions. The negative values of ΔG^0 as seen in Table 2 indicate that the interaction between the bioactives (QUE and BBR) and mucin was spontaneous. The negative and positive values of ΔH^0 and ΔS^0 respectively describe the formation of the mucin−bioactive complex, suggesting that electrostatic/ionic forces of interaction are predominantly involved in the stabilization of the mucin−bioactive complex. Notably, the magnitude of ΔS^0 was greater than that of ΔH^0 in both cases, indicating that the mucin−bioactive interactions are entropy-driven and not enthalpy-driven.[49]

CD spectroscopy is a powerful tool to investigate the protein conformation in solution during the association of proteins with other ligands. The increase in the negative band indicates that the structure of the mucin−bioactive complex is more compact than that of pure mucin and thus is consistent with previous reports.[50] Analysis of the CD spectra using BeStSel[51] revealed that the random coil content of mucin decreases in the presence of QUE and BBR, suggesting that the compactness of the protein increases after binding with the bioactive molecules (Table 3). The structural changes detected CD spectrum are in good conformity with MD simulations and also coincided with the molecular docking analysis.[32,36,48,52] Docking analysis with both the mucin sequence (PDB ID: 7PP6 and 6RBF) showed similar modes of interaction *viz*, electrostatic and ionic interactions are dominant in both systems, whereas hydrophobic interactions were also crucial in the binding process. These findings supported the results from thermodynamic parameter analysis from the temperature-dependent fluorescence study. Our results on the cobinding of both the bioactive (Figure S27) suggest that QUE and BBR can co-associate with mucin simultaneously and the association is enhanced by the other compound (Table S4). However, the binding affinity of bioactives almost remains unaffected within the studied pH range.

Biological macromolecules evolve and function within highly crowded/dense intracellular or extracellular environments and therefore the addition of crowding agents should become as routine as controlling temperature, and pH in *in vitro* protein−drug interaction experiments. Our results show that the binding stoichiometry value (n) between mucin and bioactives decreased (2:1) in the presence of crowding molecules in comparison with that in a dilute buffer system (Table 5) which is also evident from the drug release study. However, in the presence of a crowded environment, the mucin−bioactive complex shows a higher K_b value than that in the dilute buffer system and this may be due to strong binding interactions between the bioactive within the two protein residues. The change in binding stoichiometry may be due to the alternation in the protein structure in crowded environments, which is evident from our CD spectroscopic studies. Figure S26 shows that in the presence of crowders, mucin adopts a more compact structure than in a dilute buffer system, resulting in a change in binding stoichiometry.

Understanding the drug release in vitro will aid in understanding the potential drug accumulation and distribution within the cell. As evident from Figure 6, compared with the free bioactive, which exhibited a striking burst release (∼95% of the total drug was released within 16 h), the mucin−bioactive complex exhibited sustained drug release characteristics, further confirming the binding of bioactive with mucin. In comparison with the mucin−bioactive complex in a dilute buffer, a shorter time was required for the release of the bioactive from the complex in crowded media, demonstrating that the bound bioactive was released faster in a crowded environment. This is a direct consequence of the lower binding stoichiometry (2:1) in the presence of a crowding agent in comparison with that in a dilute buffer, where the binding stoichiometry is 1:1. Therefore our results raise the intriguing possibility of using mucin as a multidrug carrier at the same time, and paving the path for future refinement of mucin as a drug delivery system *in vivo*.

CONCLUSIONS

The study of the interaction of drugs with proteins is critically important to understand the pharmacokinetic and pharmacodynamic properties of drugs, including the optimization of their adsorption−distribution−metabolism−elimination profiles as well as any toxic side effects. However, such interactions are often complex in nature and therefore warrant meticulous investigation of the drug-protein interactions to achieve molecular-level interpretation. Herein, the detailed interaction behaviors of two different classes of bioactive (BBR and QUE) with mucin were investigated in both a dilute buffer and in the presence of a crowded environment using various spectroscopic and computational techniques. Steady-state UV−vis and fluorescence spectroscopy showed that both the bioactive bind with mucin while the CD spectroscopic study implied these bioactive induced a marginal alteration in the secondary structure of mucin. Computational analysis and thermodynamic parameters revealed that electrostatic/ionic interaction forces played a major role in the binding process of the mucin−bioactive complex while hydrophobic forces play a major role in stabilizing the complex. The molecular docking results indicated the preferred binding site of the bioactive within the D3 domain of mucin. pH-dependent studies showed a slight decrease in the binding of the bioactive with mucin because of the structural changes in the protein. Furthermore, the drug binding and release study in a crowded environment aided the interpretation of the bioactive absorption and distribution processes *in vivo*, which could be helpful in explaining the structure−activity relationship (SAR) of new therapeutic molecules that identify mucin as a therapeutic target.

ASSOCIATED CONTENT

Supporting Information

The Supporting Information is available free of charge at https://pubs.acs.org/doi/10.1021/acs.langmuir.2c03268.

https://doi.org/10.1021/acs.langmuir.2c03268
Langmuir 2023, 39, 4589−4600

Details of the inner filter effect, absorption spectra, and double-logarithmic plots of mucin−QUE and mucin−BBR complexes; temperature-dependent fluorescence spectra, SV plot, and double-logarithmic plot; FRET study; details molecular docking analysis with D1D2D3 domain of mucin (PDB ID: 7PP6) and D3 domain of mucin (PDB ID: 6RBF); details of MD simulation using GROMACS for mucin (PDB ID: 7PP6); details of MD simulation using Desmond tool for the D3 domain of mucin (PDB ID: 6RBF); pH-dependent fluorescence spectra, SV plot, and double-logarithmic plot; fluorescence spectra in crowded medium, double-logarithmic plot and far-UV CD spectra; bioactive cobinding fluorescence spectra; and double-logarithmic plot and binding parameters (PDF)

AUTHOR INFORMATION

Corresponding Author

Surajit Rakshit − *Department of Chemistry, Institute of Science, Banaras Hindu University, Varanasi, Uttar Pradesh 221005, India;* orcid.org/0000-0002-2739-4404; Email: srakshit.chem@bhu.ac.in

Authors

Komal Kumari − *Department of Chemistry, Institute of Science, Banaras Hindu University, Varanasi, Uttar Pradesh 221005, India*

Avinash Kumar − *Department of Pharmaceutical Chemistry, Manipal College of Pharmaceutical Sciences, Manipal, Karnataka 576104, India;* orcid.org/0000-0003-3815-1050

Ahamad Tamanna Manjur − *Department of Chemistry, Institute of Science, Banaras Hindu University, Varanasi, Uttar Pradesh 221005, India*

Complete contact information is available at: https://pubs.acs.org/10.1021/acs.langmuir.2c03268

Notes

The authors declare no competing financial interest.

ACKNOWLEDGMENTS

K.K. thanks ICMR for offering the Senior Research Fellowship (Lr. No. BMI/11(98)/2020). A.T.M. thanks SERB India for their financial support. S.R. wishes to acknowledge the SERB, Govt. of India (File no. ECR/2018/001329), and BHU, Varanasi, for providing the seed grant under the IoE scheme (Dev. Scheme No. 6031). The authors also acknowledge the Department of Chemistry and Central Discovery Centre, BHU for their in-house support.

REFERENCES

(1) Brown, T. D.; Whitehead, K. A.; Mitragotri, S. Materials for oral delivery of proteins and peptides. *Nat. Rev. Mater.* **2020**, *5*, 127−148.

(2) Dahlgren, D.; Lennernäs, H. Intestinal Permeability and Drug Absorption: Predictive Experimental, Computational and In Vivo Approaches. *Pharmaceutics* **2019**, *11*, No. 411.

(3) Murgia, X.; Loretz, B.; Hartwig, O.; Hittinger, M.; Lehr, C.-M. The role of mucus on drug transport and its potential to affect therapeutic outcomes. *Adv. Drug Delivery Rev.* **2018**, *124*, 82−97.

(4) Khanvilkar, K.; Donovan, M. D.; Flanagan, D. R. Drug transfer through mucus. *Adv. Drug Delivery Rev.* **2001**, *48*, 173−193.

(5) Reis, C. A.; Osorio, H.; Silva, L.; Gomes, C.; David, L. Alterations in glycosylation as biomarkers for cancer detection. *J. Clin. Pathol.* **2010**, *63*, 322−329.

(6) Adamczyk, B.; Tharmalingam, T.; Rudd, P. M. Glycans as cancer biomarkers. *Biochim. Biophys. Acta, Gen. Subj.* **2012**, *1820*, 1347−1353.

(7) Boegh, M.; García-Díaz, M.; Müllertz, A.; Nielsen, H. M. Steric and interactive barrier properties of intestinal mucus elucidated by particle diffusion and peptide permeation. *Eur. J. Pharm. Biopharm.* **2015**, *95*, 136−143.

(8) Johansson, M. E. V.; Larsson, J. M. H.; Hansson, G. C. The two mucus layers of colon are organized by the MUC2 mucin, whereas the outer layer is a legislator of host−microbial interactions. *Proc. Natl. Acad. Sci. U.S.A.* **2011**, *108*, 4659−4665.

(9) Hansson, G. C.; Johansson, M. E. V. The inner of the two Muc2 mucin-dependent mucus layers in colon is devoid of bacteria. *Gut Microbes* **2010**, *1*, 51−54.

(10) Xu, Q.; Ensign, L. M.; Boylan, N. J.; Schön, A.; Gong, X.; Yang, J.-C.; Lamb, N. W.; Cai, S.; Yu, T.; Freire, E.; Hanes, J. Impact of Surface Polyethylene Glycol (PEG) Density on Biodegradable Nanoparticle Transport in Mucus ex Vivo and Distribution in Vivo. *ACS Nano* **2015**, *9*, 9217−9227.

(11) Huang, J. X.; Blaskovich, M. A. T.; Pelingon, R.; Ramu, S.; Kavanagh, A.; Elliott, A. G.; Butler, M. S.; Montgomery, A. B.; Cooper, M. A. Mucin Binding Reduces Colistin Antimicrobial Activity. *Antimicrob. Agents Chemother.* **2015**, *59*, 5925−5931.

(12) Butnarasu, C.; Barbero, N.; Pacheco, D.; Petrini, P.; Visentin, S. Mucin binding to therapeutic molecules: The case of antimicrobial agents used in cystic fibrosis. *Int. J. Pharm.* **2019**, *564*, 136−144.

(13) Pontremoli, C.; Barbero, N.; Viscardi, G.; Visentin, S. Mucin−drugs interaction: The case of theophylline, prednisolone and cephalexin. *Bioorg. Med. Chem.* **2015**, *23*, 6581−6586.

(14) Yu, X.; Liu, H.; Yang, Y.; Lu, S.; Yao, Q.; Yi, P. The investigation of the interaction between Oxymetazoline hydrochloride and mucin by spectroscopic approaches. *Spectrochim. Acta, Part A* **2013**, *103*, 125−129.

(15) Habtemariam, S. Berberine pharmacology and the gut microbiota: A hidden therapeutic link. *Pharmacol. Res.* **2020**, *155*, No. 104722.

(16) Liu, Y.; Yu, H.; Zhang, C.; Cheng, Y.; Hu, L.; Meng, X.; Zhao, Y. Protective effects of berberine on radiation-induced lung injury via intercellular adhesion molecular-1 and transforming growth factor-beta-1 in patients with lung cancer. *Eur. J. Cancer* **2008**, *44*, 2425−2432.

(17) Hu, Y.-J.; Liu, Y.; Xiao, X.-H. Investigation of the Interaction between Berberine and Human Serum Albumin. *Biomacromolecules* **2009**, *10*, 517−521.

(18) Hsieh, Y.-S.; Kuo, W.-H.; Lin, T.-W.; Chang, H.-R.; Lin, T.-H.; Chen, P.-N.; Chu, S.-C. Protective Effects of Berberine against Low-Density Lipoprotein (LDL) Oxidation and Oxidized LDL-Induced Cytotoxicity on Endothelial Cells. *J. Agric. Food Chem.* **2007**, *55*, 10437−10445.

(19) Bjorklund, J. A.; Frenzel, T.; Rueffer, M.; Kobayashi, M.; Mocek, U.; Fox, C.; Beale, J. M.; Groeger, S.; Zenk, M. H.; Floss, H. G. Cryptic stereochemistry of berberine alkaloid biosynthesis. *J. Am. Chem. Soc.* **1995**, *117*, 1533−1545.

(20) Srivastava, A. K. Inhibition of phosphorylase kinase, and tyrosine protein kinase activities by quercetin. *Biochem. Biophys. Res. Commun.* **1985**, *131*, 1−5.

(21) Boege, F.; Straub, T.; Kehr, A.; Boesenberg, C.; Christiansen, K.; Andersen, A.; Jakob, F.; Köhrle, J. Selected Novel Flavones Inhibit the DNA Binding or the DNA Religation Step of Eukaryotic Topoisomerase I (*). *J. Biol. Chem.* **1996**, *271*, 2262−2270.

(22) Sengupta, B.; Sengupta, P. K. The interaction of quercetin with human serum albumin: a fluorescence spectroscopic study. *Biochem. Biophys. Res. Commun.* **2002**, *299*, 400−403.

(23) Macha, M. A.; Krishn, S. R.; Jahan, R.; Banerjee, K.; Batra, S. K.; Jain, M. Emerging potential of natural products for targeting

mucins for therapy against inflammation and cancer. *Cancer Treat. Rev.* **2015**, *41*, 277−288.
(24) Lee, C. J.; Lee, J. H.; Seok, J. H.; Hur, G. M.; Park, Y. C.; Seol, I. C.; Kim, Y. H. Effects of Baicalein, Berberine, Curcumin and Hesperidin on Mucin Release from Airway Goblet Cells. *Planta Med.* **2003**, *69*, 523−526.
(25) Madhavi Sastry, G.; Adzhigirey, M.; Day, T.; Annabhimoju, R.; Sherman, W. Protein and ligand preparation: parameters, protocols, and influence on virtual screening enrichments. *J. Comput.-Aided Mol. Des.* **2013**, *27*, 221−234.
(26) Javitt, G.; Calvo, M. L. G.; Albert, L.; Reznik, N.; Ilani, T.; Diskin, R.; Fass, D. Intestinal Gel-Forming Mucins Polymerize by Disulfide-Mediated Dimerization of D3 Domains. *J. Mol. Biol.* **2019**, *431*, 3740−3752.
(27) Kumar, A.; Rajappan, R.; Kini, S. G.; Rathi, E.; Dharmarajan, S.; Sreedhara Ranganath Pai, K. e-Pharmacophore model-guided design of potential DprE1 inhibitors: synthesis, in vitro antitubercular assay and molecular modelling studies. *Chem. Pap.* **2021**, *75*, 5571−5585.
(28) Friesner, R. A.; Murphy, R. B.; Repasky, M. P.; Frye, L. L.; Greenwood, J. R.; Halgren, T. A.; Sanschagrin, P. C.; Mainz, D. T. Extra precision glide: docking and scoring incorporating a model of hydrophobic enclosure for protein-ligand complexes. *J. Med. Chem.* **2006**, *49*, 6177−6196.
(29) Berendsen, H. J. C.; van der Spoel, D.; van Drunen, R. GROMACS: A message-passing parallel molecular dynamics implementation. *Comput. Phys. Commun.* **1995**, *91*, 43−56.
(30) Bowers, K. J.; Chow, D. E.; Xu, H.; Dror, R. O.; Eastwood, M. P.; Gregersen, B. A.; Klepeis, J. L.; Kolossvary, I.; Moraes, M. A.; Sacerdoti, F. D.; Salmon, J. K.; Shan, Y.; Shaw, D. E. In *Scalable Algorithms for Molecular Dynamics Simulations on Commodity Clusters, SC '06*, Proceedings of the 2006 ACM/IEEE Conference on Supercomputing, 11−17 Nov. 2006; pp 43−43, 44−43.
(31) Li, J.; Abel, R.; Zhu, K.; Cao, Y.; Zhao, S.; Friesner, R. A. The VSGB 2.0 model: a next generation energy model for high resolution protein structure modeling. *Proteins* **2011**, *79*, 2794−2812.
(32) Maurya, N.; Maurya, J. K.; Singh, U. K.; Dohare, R.; Zafaryab, M.; Moshahid Alam Rizvi, M.; Kumari, M.; Patel, R. In Vitro Cytotoxicity and Interaction of Noscapine with Human Serum Albumin: Effect on Structure and Esterase Activity of HSA. *Mol. Pharm.* **2019**, *16*, 952−966.
(33) Rabbani, G.; Lee, E. J.; Ahmad, K.; Baig, M. H.; Choi, I. Binding of Tolperisone Hydrochloride with Human Serum Albumin: Effects on the Conformation, Thermodynamics, and Activity of HSA. *Mol. Pharm.* **2018**, *15*, 1445−1456.
(34) Khashkhashi-Moghadam, S.; Ezazi-Toroghi, S.; Kamkar-Vatanparast, M.; Jouyaeian, P.; Mokaberi, P.; Yazdyani, H.; Amiri-Tehranizadeh, Z.; Reza Saberi, M.; Chamani, J. Novel perspective into the interaction behavior study of the cyanidin with human serum albumin-holo transferrin complex: Spectroscopic, calorimetric and molecular modeling approaches. *J. Mol. Liq.* **2022**, *356*, No. 119042.
(35) Marjani, N.; Dareini, M.; Asadzade-Lotfabad, M.; Pejhan, M.; Mokaberi, P.; Amiri-Tehranizadeh, Z.; Saberi, M. R.; Chamani, J. Evaluation of the binding effect and cytotoxicity assay of 2-Ethyl-5-(4-methylphenyl) pyramido pyrazole ophthalazine trione on calf thymus DNA: spectroscopic, calorimetric, and molecular dynamics approaches. *Luminescence* **2022**, *37*, 310−322.
(36) Paul, B. K.; Ghosh, N.; Mukherjee, S. Binding Interaction of a Prospective Chemotherapeutic Antibacterial Drug with β-Lactoglobulin: Results and Challenges. *Langmuir* **2014**, *30*, 5921−5929.
(37) Madsen, J. B.; Pakkanen, K. I.; Lee, S. Investigation of the Thermostability of Bovine Submaxillary Mucin (BSM) and its Impact on Lubrication. *APCBEE Procedia* **2013**, *7*, 21−26.
(38) Zappone, B.; Patil, N. J.; Madsen, J. B.; Pakkanen, K. I.; Lee, S. Molecular Structure and Equilibrium Forces of Bovine Submaxillary Mucin Adsorbed at a Solid−Liquid Interface. *Langmuir* **2015**, *31*, 4524−4533.
(39) Kumar, A.; Rathi, E.; Kini, S. G. Identification of E6 Inhibitors Employing Energetically Optimized Structure-Based Pharmacophore Modelling, Ligand Docking and Molecular Dynamics Simulations Studies. *ChemistrySelect* **2019**, *4*, 10701−10708.
(40) Bhaskar, K. R.; Garik, P.; Turner, B. S.; Bradley, J. D.; Bansil, R.; Stanley, H. E.; LaMont, J. T. Viscous fingering of HCI through gastric mucin. *Nature* **1992**, *360*, 458−461.
(41) Nordman, H.; Borén, T.; Davies, J. R.; Engstrand, L.; Carlstedt, I. pH-dependent binding of *Helicobacter pylori* to pig gastric mucins. *FEMS Immunol. Med. Microbiol.* **1999**, *24*, 175−181.
(42) Cao, X.; Bansil, R.; Bhaskar, K. R.; Turner, B. S.; LaMont, J. T.; Niu, N.; Afdhal, N. H. pH-Dependent Conformational Change of Gastric Mucin Leads to Sol-Gel Transition. *Biophys. J.* **1999**, *76*, 1250−1258.
(43) Bhaskar, K. R.; Gong, D. H.; Bansil, R.; Pajevic, S.; Hamilton, J. A.; Turner, B. S.; LaMont, J. T. Profound increase in viscosity and aggregation of pig gastric mucin at low pH. *Am. J. Physiol.: Gastrointest. Liver Physiol.* **1991**, *261*, G827−G832.
(44) Saha, R.; Rakshit, S.; Verma, P. K.; Mitra, R. K.; Pal, S. K. Protein−cofactor binding and ultrafast electron transfer in riboflavin binding protein under the spatial confinement of nanoscopic reverse micelles. *J. Mol. Recognit.* **2013**, *26*, 59−66.
(45) Rakshit, S.; Saha, R.; Verma, P. K.; Mitra, R. K.; Pal, S. K. Ultrafast electron transfer in riboflavin binding protein in macromolecular crowding of nano-sized micelle. *Biochimie* **2012**, *94*, 2673−2680.
(46) Verma, P. K.; Rakshit, S.; Mitra, R. K.; Pal, S. K. Role of hydration on the functionality of a proteolytic enzyme α-chymotrypsin under crowded environment. *Biochimie* **2011**, *93*, 1424−1433.
(47) Rakshit, S.; Saha, R.; Pal, S. K. Modulation of environmental dynamics at the active site and activity of an enzyme under nanoscopic confinement: Subtilisin carlsberg in anionic AOT reverse micelle. *J. Phys. Chem. B* **2013**, *117*, 11565−11574.
(48) Suo, Z.; Xiong, X.; Sun, Q.; Zhao, L.; Tang, P.; Hou, Q.; Zhang, Y.; Wu, D.; Li, H. Investigation on the Interaction of Dabrafenib with Human Serum Albumin Using Combined Experiment and Molecular Dynamics Simulation: Exploring the Binding Mechanism, Esterase-like Activity, and Antioxidant Activity. *Mol. Pharm.* **2018**, *15*, 5637−5645.
(49) Russi, M.; Cavalieri, G.; Marson, D.; Laurini, E.; Pricl, S. Binding of the B-Raf Inhibitors Dabrafenib and Vemurafenib to Human Serum Albumin: A Biophysical and Molecular Simulation Study. *Mol. Pharm.* **2022**, *19*, 1619−1634.
(50) Nikogeorgos, N.; Patil, N. J.; Zappone, B.; Lee, S. Interaction of porcine gastric mucin with various polycations and its influence on the boundary lubrication properties. *Polymer* **2016**, *100*, 158−168.
(51) Micsonai, A.; Wien, F.; Bulyáki, É.; Kun, J.; Moussong, É.; Lee, Y.-H.; Goto, Y.; Réfrégiers, M.; Kardos, J. BeStSel: a web server for accurate protein secondary structure prediction and fold recognition from the circular dichroism spectra. *Nucleic Acids Res.* **2018**, *46*, W315−W322.
(52) Karthikeyan, S.; Bharanidharan, G.; Ragavan, S.; Kandasamy, S.; Chinnathambi, S.; Udayakumar, K.; Mangaiyarkarasi, R.; Suganya, R.; Aruna, P.; Ganesan, S. Exploring the Binding Interaction Mechanism of Taxol in β-Tubulin and Bovine Serum Albumin: A Biophysical Approach. *Mol. Pharm.* **2019**, *16*, 669−681.

https://doi.org/10.1021/acs.langmuir.2c03268
Langmuir 2023, 39, 4589−4600